Potential trace-chemical (Fe, Mn, CH_4) limitation on bacterial growth in deep sea hydrothermal vent plumes along the Southern East Pacific Rise

Dylan Vecchione

University of Washington, School of Oceanography

dylanv21@uw.edu

March 11th, 2022

Abstract: Global cycling of elements like carbon, nitrogen, and iron has a key role in maintaining the biosphere. These and other micro- and macro-nutrients undergo important reduction-oxidation and acid-base transformations in the environment. Biologically, iron (Fe) and manganese (Mn) are utilized by microbes as cofactors in many essential proteins and enzymes including nitrogenase, ferredoxin, peroxidase, cytochromes, and phosphotransferase. These elements (most notably Fe) can often limit microbial growth in large regions of the ocean due to their trace environmental concentrations, structural bioavailability, or competitive microbial uptake and utilization. This can impact key ecosystem processes, including chemosynthetic carbon fixation at hydrothermal vents, nitrogen species reduction, and metabolic electron transport. Here I used flow cytometry measurements (FCM) to quantify bacteria and archaea from hydrothermal vent plumes along the Southern East Pacific Rise in September-November 2021. I compared patterns in microbial abundance with total dissolvable Fe concentrations (predominantly Fe^{3+}, including dissolved and labile particulate Fe) and other key chemicals like Mn and methane (CH_4) at the same locations. I hypothesized that hydrothermal sites with higher chemical concentrations would also have higher microbial abundance. I found that bacterial abundance is positively related to trace-concentration of Fe below 400nM (r^2_{Fe}= 0.67), and that similar relationships exist with trace CH_4 and Mn concentrations (r^2_{CH4} = 0.55; r^2_{Mn} = 0.51). These findings suggest that microbial abundances in vent plumes can be partially explained by trace metal and methane distributions. Further research is required to disentangle whether these substrates covary with other biochemical controls on microbial growth and metabolism (like sulfide nutrients) in these dynamic environments.

Project Summary: Global cycling of elements like carbon, nitrogen, and iron play key roles in the maintenance of Earth's habitability. These elements participate in important chemical reactions in the environment and are utilized by microbes as components in molecules involved in key organism and ecosystem processes. These elements are often limiting factors on growth for marine microorganisms, which is significant due to the organisms' roles in processes like nutrient recycling, carbon burial, oxygen production, and establishing the foundation of the food-web. Iron is one key nutrient that limits growth in many regions of the global oceans. One mechanism to explain the oceanic-scale distribution of iron is the interaction with biologically produced molecules which might prevent or control utilization of iron by marine microorganisms. To better understand how iron impacts bacterial populations and potentially limits growth, an international research team lead by the University of Washington measured concentrations of key chemicals in seawater and microbial abundance at deep-sea volcanos in the South Pacific, located approximately 3000 nautical miles off the Peruvian coastline, during a research period between September and November 2021. I hypothesized that sites with higher chemical concentrations would also have higher microbial abundance because of iron's tendency to limit growth. I found that bacterial abundance is most strongly related to low iron concentration between 0 to 400nM, and that similar relationships exist for Manganese (Mn) and Methane (CH_4). This work suggests that these trace chemicals might have a role in controlling microbial growth in these dynamic ecosystems, and further research is required to determine which nutrients are actively limiting microbial growth.

Introduction:

Global biogeochemical cycles of elements like carbon, nitrogen, and iron supply the environment with key nutrients required for life. Iron in the ocean is a nutrient that can influence growth of microorganisms since it is an essential cofactor in many biomolecules, influencing cellular processes like photosynthesis, respiration, and nitrogen fixation (Twining and Baines 2013). As a result, the concentrations and bioavailability of iron can regulate microbiology in some regions of the ocean, which is significant because microorganisms play a pivotal role in global biosphere dynamics (Zhao and Bajic 2015). Iron limitation is the phenomenon whereby microbial growth or bioproductivity of a region is limited by the concentration of iron, rather than other key nutrients. This often manifests where the concentration of other key nutrients like nitrate (which is itself often limiting) are high, like in the Southern Ocean, North Pacific, Northeast Atlantic, and the Equatorial Pacific (Moore et al. 2013; Boyd et al. 2012; Birchill et al. 2019). These regions have sufficient concentrations of macronutrients (nitrate, phosphate, silicate) to support metabolic and biosynthetic demands, but lack enough iron to support microbial biochemical demands and draw down of the other in situ macronutrients. The iron limitation in the polar latitudes is often driven by diminished aeolian dust transport to the surface ocean. The Equatorial Pacific often experiences iron limitation due to excess macronutrient input fluxes caused by unique circulatory dynamics like significant upwelling of nutrient rich deep waters. Although dissolved iron concentrations limit productivity in large areas of the surface ocean, the dissolved iron concentrations do not increase significantly with depth, and there is no accumulation of dissolved iron in the oldest deep waters of the North Pacific due to the short residence time of dissolved iron in seawater (Tagliabue et al. 2017).

Hydrothermal vent fluids are rich in iron, and so understanding the fluxes, sources and sinks, the bioavailability, and the vent's internal cycling of iron is key to understanding its global impacts (Statham et al. 2005). Plume fluids and their chemical constituents change as the water parcels are advected off-source. Reduced elements are chemically and biologically transformed to support processes like metabolism, and their concentrations diminish as the plume advects away from its source, diffuses, and ages. This is important because the distance to the plume source and the specific composition of plume nutrients can impact the microbial community and abundance since metabolism is required to support the synthesis of biomolecules.

Understanding the mechanisms by which iron may be introduced into the deep sea and distributed throughout the basin is a key modern research focus. While it was previously assumed that iron was quantitatively removed in close proximity to the vent source, it has now been observed that appreciable levels of dissolved iron can be transported thousands of kilometers away from the ridge crest (Resing et al. 2015). One research question currently under investigation by trace-metal biogeochemical cycling researchers like the Bundy Lab at the University of Washington School of Oceanography is the role of microbially synthesized siderophores, or biogenic iron-binding molecules with a high affinity for iron, in stabilizing iron and allowing for larger scale distribution by advection. The complexation of iron by siderophores could prevent its precipitation, altering the rate of microbial uptake, retaining iron in the neutrally buoyant plume, and allowing for greater dispersion of hydrothermal iron. Since siderophores might control this distribution, an understanding of the microbial communities existing in different hydrothermal systems is important. These siderophores could also decrease the bioavailability of the hydrothermal iron to some microbes in the neutrally-buoyant plume, allowing for more iron to escape the ridge crest. Alternatively, bacteria may be actively secreting

these molecules to recycle and retain dissolved iron in the advecting plume. This understanding is hindered by our limited knowledge of marine microbial communities, with environmental metagenomic analyses showing that 97.9% of bacterial operational taxonomic units (OTUs: genetic designations similar to species) remain unknown (Waschulin et al. 2021).

To investigate the first-order relationship between microbial community and iron concentration, measurements of cell abundance (using flow cytometry measurements: FCM) were collected aboard cruise RR2106 and compared to iron, manganese, and methane measurements collected at the same sites. I assessed how microbiological abundance might be impacted by iron availability (concentration) and what the distributions might suggest about how biological activity is altering the chemical dynamics of hydrothermal iron inputs. This FCM work seeks to further collective understandings of the role of iron (and other trace chemicals) in controlling growth in vent plume ecosystems. Evaluation of chemical datasets collected shipboard and by the Bundy Lab at UW Oceanography will augment my biological datasets for a more complete analysis of vent characteristics, and for investigations into bacterial relationships with trace iron concentrations.

I hypothesize that hydrothermal sites with higher iron concentrations will also have higher bacterial abundance than background deep ocean samples, and that this pattern will be consistent for other key nutrients. I propose this because iron (and other key chemicals) can limit bacterial growth in some environments, especially at trace concentrations. Additionally, I hypothesize that sites with higher Oxidation-Reduction Potential signals will also have higher microbial abundance, because the ORP signal is controlled by reducing elements that can be utilized in microbial metabolism.

Methods:

Sample collection occurred on NSF-funded research cruise Resing RR2106 from September 12, 2021-November 8, 2021, an expedition aboard the UNOLS Research Vessel R/V *Roger Revelle* to the Southern East Pacific Rise (SEPR). Samples were collected from three discrete ridge segments spanning from 16ºS to 18ºS, with additional off-axis sampling occurring throughout the region from 15ºN to 18ºS (Figure 1).

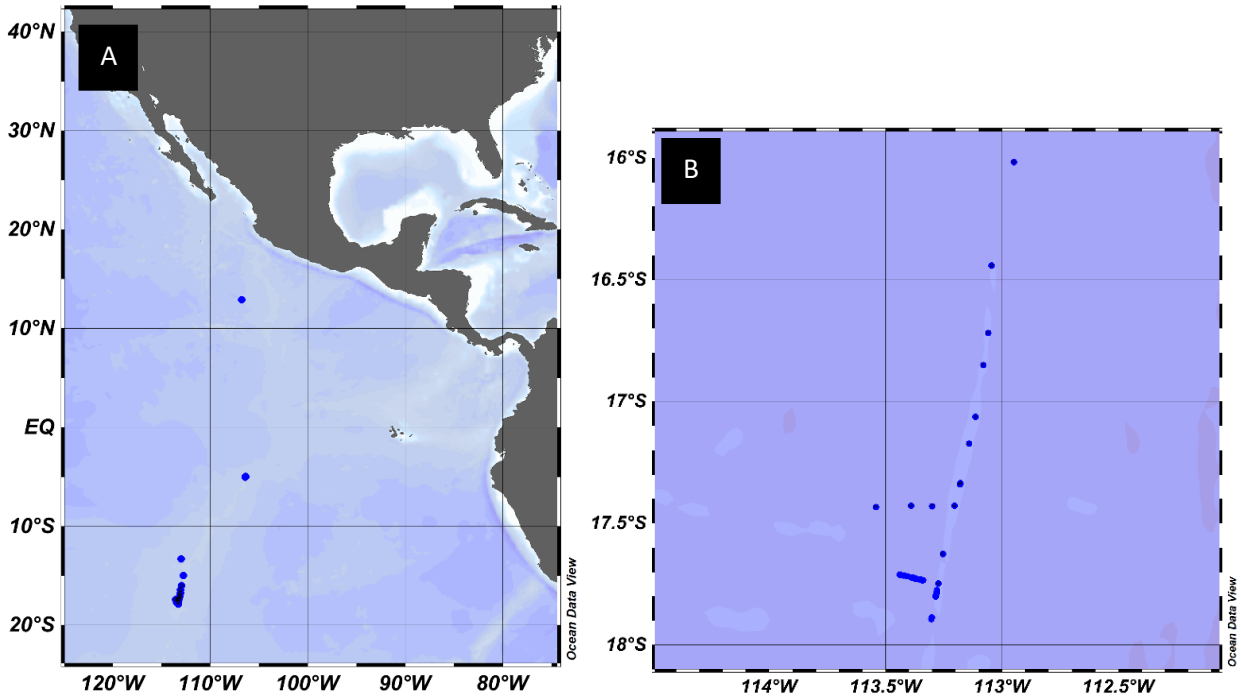

Figure 1: A) *On- and Off- axis sampling sites for FCM along the East Pacific and Southern East Pacific Rise (SEPR). Blue Dots denote station locations where sampling occurred. Background color contours show rough bathymetry, where darker blues denote deeper terrain.* ***B)*** *Focused region of primary sampling on the SEPR for On- and Cross-axis segments between latitudes of 16S and 18S. Background color contours in lighter blue show the ridge axis (shallower; following N/S sampling locations) and additional off-axis bathymetric features.*

Woods Hole Oceanographic Institute's Autonomous Underwater Vehicle SENTRY was deployed along each ridge segment with an Oxidative-Reductive Potential (ORP) sensor, detecting possible locations of hydrothermal activity. Each promising location (denoted by an ORP signal) was probed with an exploratory Hydrothermal Cast (hydrocast).

Hydrocasts utilized NOAA Pacific Marine Environmental Laboratory's (PMEL) custom-built hydrothermal rosette, and one to seven key depths per site were identified and subsampled for cell abundance measurements (two to four depths for metagenomics) based on downcast conductivity, temperature, depth (CTD), Light Scatter Sensor (LSS), and ORP data. LSS signatures were used as a proxy for particle concentration, which indicated a hydrothermal plume when turbidity peaked within a discrete depth-band in the water column. ORP was used to determine the redox potential, which indicated the age of the plume signal, because newer plume fluids contain elements that are more reducing (e.g. Fe^{2+}, H_2) and are not yet chemically nor biologically transformed to higher oxidation states. CTD measurements were used to assess the water parcel physical characteristics, specifically to determine potential density (for plume buoyancy) and temperature anomalies associated with fresh or buoyant hydrothermal plumes. I assessed the live data stream in the vessel's computer lab during the downcast and determined a sampling regime. For each site, I attempted to capture the unique plume features where the potential for biologically and chemically relevant water parcels was highest. I prepared vials for sample collection during the upcast to be ready for rosette retrieval and time sensitive subsampling. Background samples were also collected, often at 2200m depth because these depths were well above any possible hydrothermal plume signals while also still being in the deep ocean.

I subsampled off the PMEL Hydrothermal Rosette, and 225µL of raw seawater was transferred into Nalgene Cryovials with 25µL aliquots of formalin (10% final concentration by volume of formaldehyde in MilliQ) to fix the sample. Samples were processed following ship-board sterile technique before cryogenic preservation at -80C. In parallel, metagenomes were sampled and filtered on Isopore 0.2µm polycarbonate 47mm filters. Water volume and filtration duration were

recorded to inform the extraction and sequencing steps. FCM and metagenomic samples were transported back to UW's Center for Environmental Genomics (CEG) in a liquid nitrogen dry shipper (dewar) for processing on a GUAVA Technologies easyCyte flow cytometer. Flow cytometers use spectroscopy and fluorescence to determine cell density and cell characteristics. Samples were stored in the CEG -80C freezer, and thawed once ready for processing. Samples were individually plated on a 96 well plate. First 3µL of SYBR Green nucleic acid (genetic) stain was pipetted into each well using a Rainin P10 multichannel pipettor. Then 150µL of sample was added to the well and mixed by gently drawing and ejecting the sample and SYBR mixture 3x per well using the Rainin single channel P200 pipettor. The SYBR and sample mixture was allowed to incubate for 30 minutes in the dark. Throughout the plating process, exposure to light was minimized, as SYBR photo-degrades. The completed plate was loaded into the GUAVA flow cytometer and run following CEG Morris Lab GUAVA protocol. Additional plates were prepared while the preceding plate ran in the GUAVA. Subsequent to this FCM analysis, metagenomes will be developed to assess the microbial community structure and genetic potential for siderophore production and uptake at various vent types at the SEPR, as well as background samples collected in the off-axis sites and above the plume depth (Genitsaris et al. 2016).

Data was processed and visualized using a combination of Ocean Data View, Excel, and Python. Analysis of descriptive statistics and trace thresholds, as well as data handling was conducted in Excel. Visualization was performed in Ocean Data View, as well as the initial assessment of geospatial patterns in preliminary chemical data. Python packages Pandas, Seaborn, Numpy and Matplotlib were employed to complement regression analysis and plotting.

Results:

Downcasts were utilized to determine the sampling regime at each station. The ORP signal from older plumes with more oxidized chemical constituents does not change from background ORP levels, ignoring variation due to sensor hysteresis, indicating a plume with minimal redox potential (Figure 2 A). Significant decreases in ORP signal indicates fresher plume fluids with reducing chemistry (Figure 2 B). The ORP signal decreased significantly at 2380m and at the 2580m (bottom depth). These voltage drops indicated young vent fluid, and active venting. The shape of the LSS signature (broad peak with respect to depth, extending to the bottom depth) indicated potential diffuse low temperature flow, or diffuse flow beneath a typical high temperature buoyant plume.

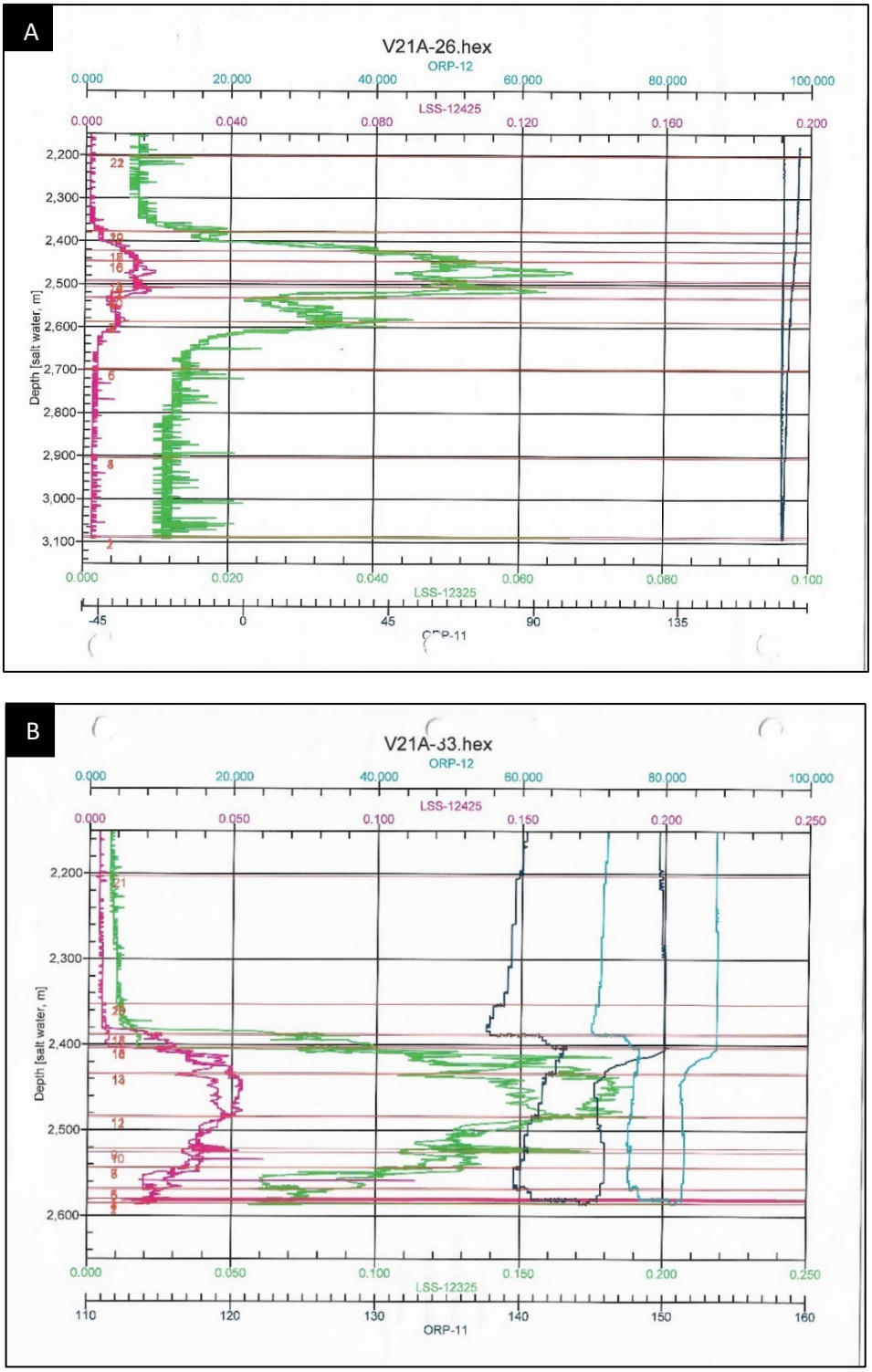

Figure 2: ***A)*** *Example downcast profile showing LSS (Green) plume signal, but no ORP (Black) signal, ignoring sensor hysteresis. This is indicative of an older plume.* ***B)*** *Downcast signature at unique diffuse flow station with significant ORP (Blue and Black) signals at 2380m and 2580m.*

Sampling and shipboard chemical analysis indicated that strong Fe and turbidity signals manifested between 16ºS to 18ºS, with the highest activity on the southernmost ridge segment between 17º30' S and 18º00' S, as shown by shipboard dissolved iron measurements and light scatter sensor (LSS; dNTU) cross sections below (Figure 3). The high dissolved iron signature between 17.5ºS and 18ºS is the focus of sampling.

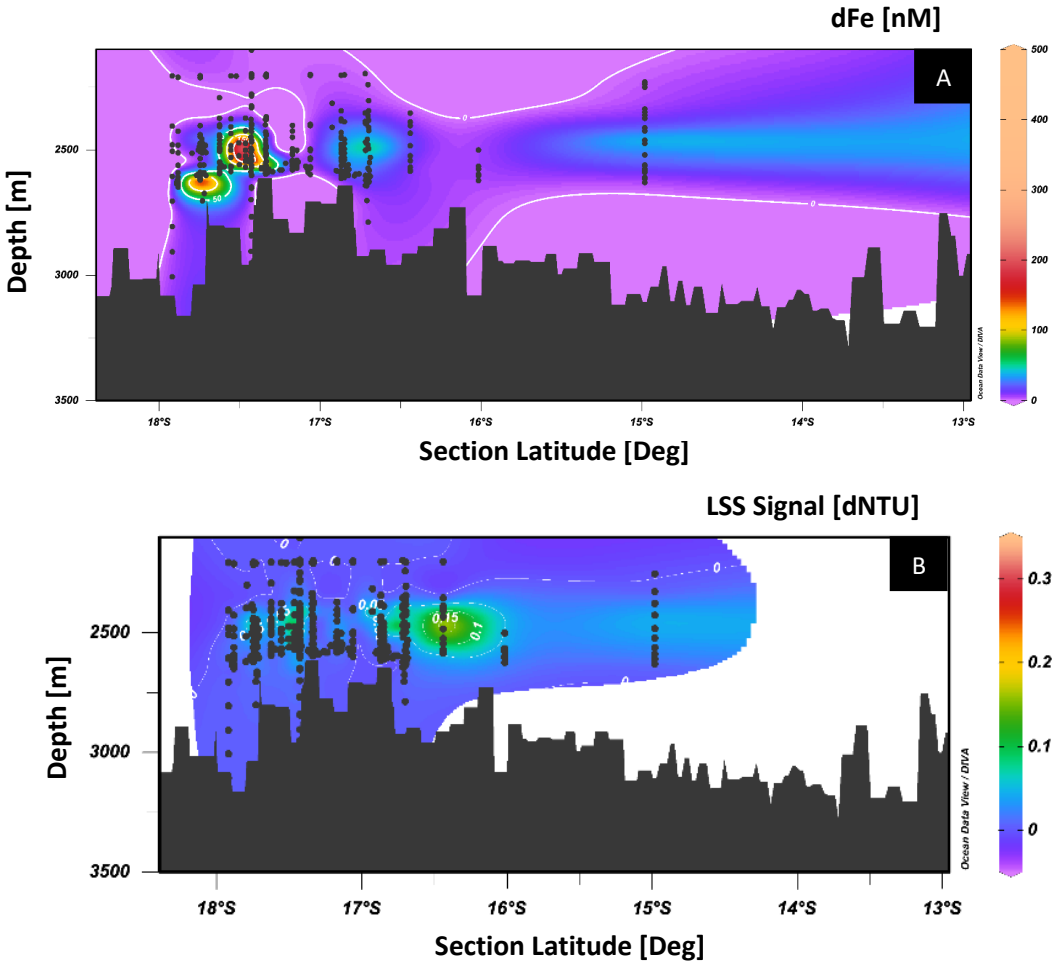

Figure 3*: Profile cross sections showing dissolved iron* ***(A)*** *and LSS (dNTU, Nepholometry Turbiditity Units;* ***B)*** *distributions along RR2106 track line from 13S to 18S. Black dots indicate discrete sampling locations, and color contours show interpolation between points.*

ORP features in downcast data determined a significant proportion of our sampling. As such, an evaluation of the predictive value of our ORP signal is important. I evaluated the visual homogeneity of the ORP signal compared to total iron (tFe) and Methane (CH4) concentrations,

where methane is used as a classical plume signature and provides a baseline for plume presence (Figure 4).

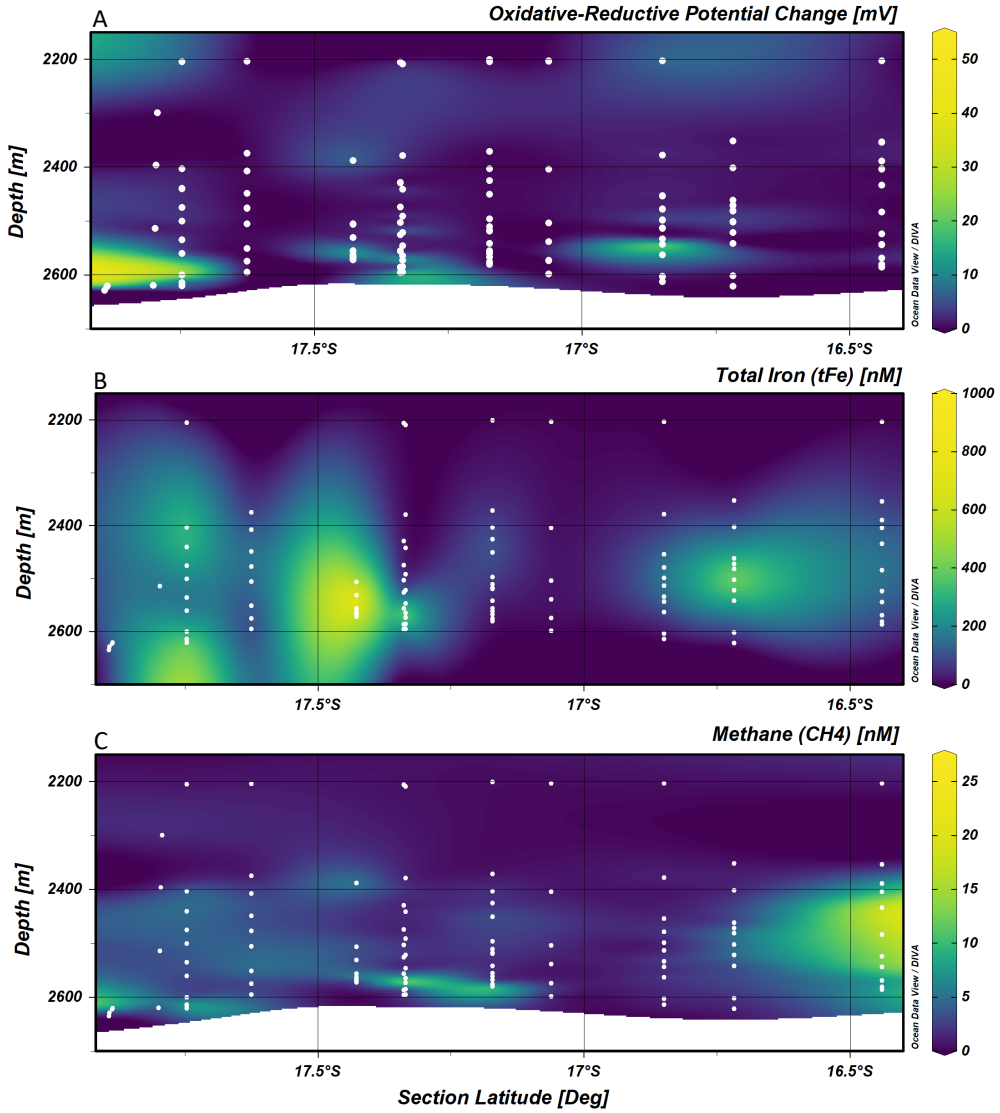

Figure 4: *Assessment of similarities between cross-section profiles from 18S to 16.35S showing change in Rosette Oxidative-Reductive Potential (ORP) signal [mV]* ***(A)****, total iron [nM]* ***(B)****, and methane [nM]* ***(C)*** *signatures. ORP signals were used to determine the sampling regime, as ORP signal is indicative of young hydrothermal plume fluid. Total iron was sampled to assess the impact of vents on marine iron input. Methane was sampled as a hydrothermal plume indicator. Iron distributions are not consistently similar to ORP nor Methane distributions, and do not seem to control ORP signal. White dots represent discrete sampling points. White regions denote the border of interpolation confidence, not bottom-depth.*

ORP signal does not overlap consistently with the total iron signature, but does share signal shape, latitude, and depth with methane signals (yellow-green regions) at 17.25S and 17.9S. This

suggests that ORP is related to plume fluids, but is not a strong predictor of total iron concentration nor bacterial abundance. No relationship between ORP and neither total iron nor bacterial abundance are found (Figure 5; $r^2_{tFe} = 0.32$; $r^2_{Bacterial} = -0.052$).

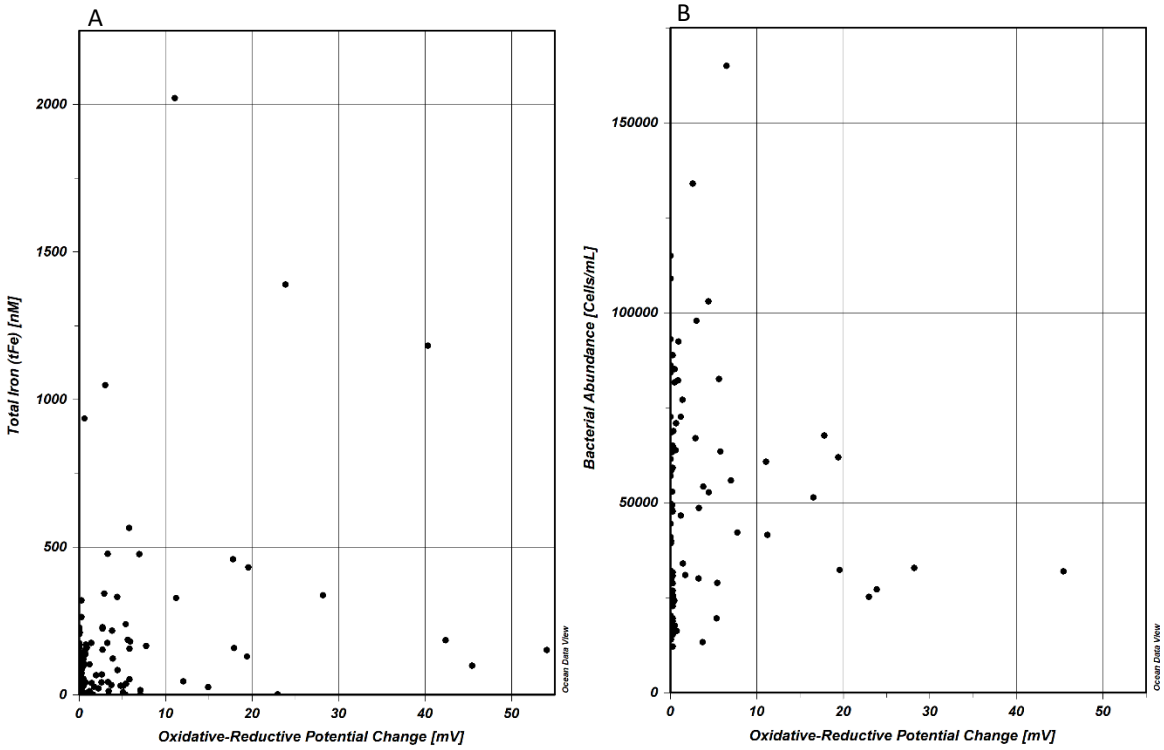

Figure 5: *Scatter plot* comparing *iron concentration with ORP change* ***(A)****, and bacterial abundance with ORP change* ***(B)****. Both relationships are not strongly related to ORP signal ($r^2_{tFe} = 0.32$; $r^2_{Bacterial} = -0.052$). A negative r^2 value indicates that the linear regression model does not fit the data trends.*

This suggests that iron output does not control ORP signal, and that ORP is not strongly predictive of bacterial abundance.

Focusing on iron and bacterial abundance specifically, profile cross sections show a higher degree of homology between signals (Figure 6).

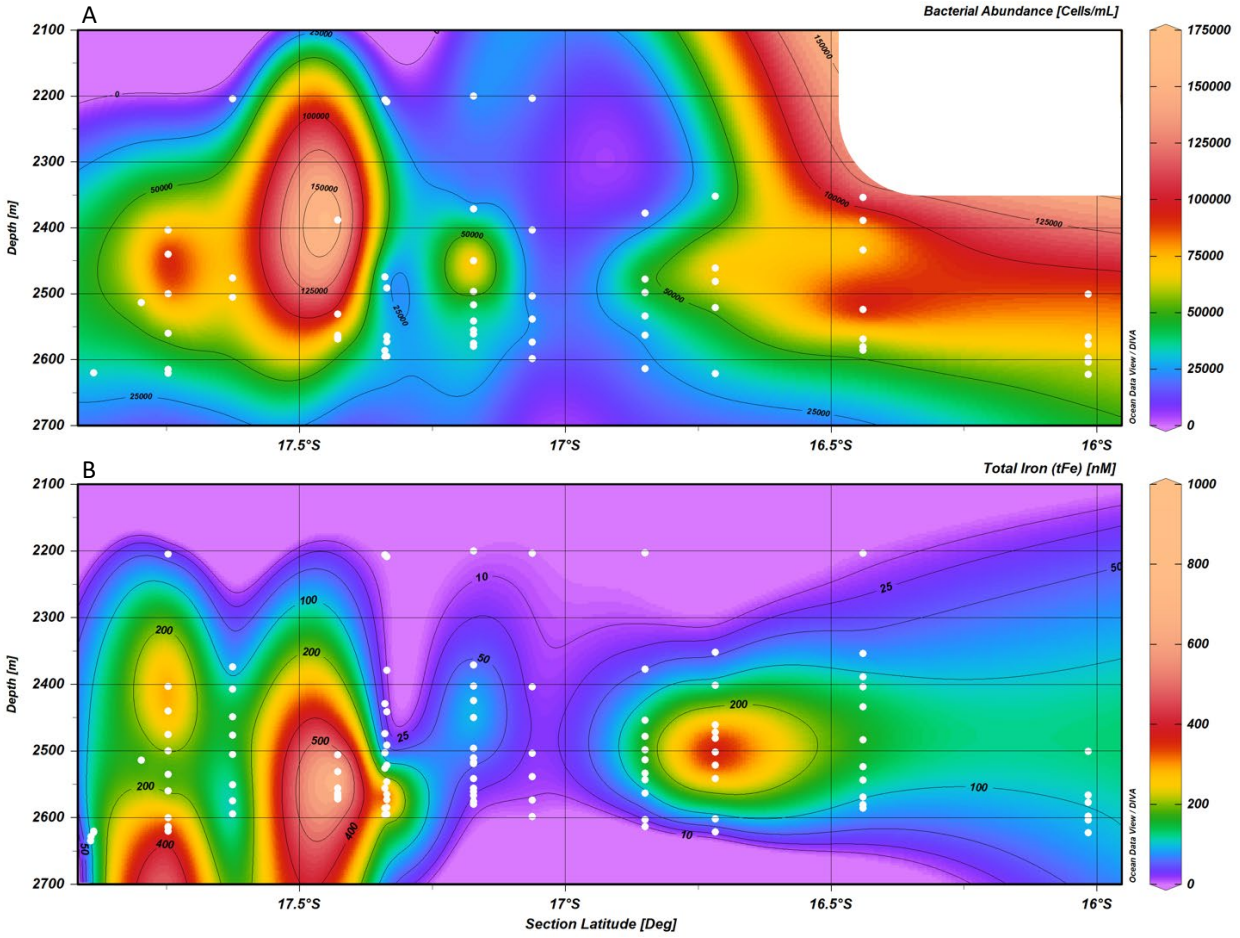

Figure 6: *Profile cross-sections along the ridge axis from 18S to 16S comparing bacterial abundance [Cells/mL]* ***(A)*** *to total iron [nM]* ***(B)****. White dots represent discrete sampling locations. White regions denote low interpolation confidence based on insufficient data.*

The profile cross sections of total iron and bacterial abundance evidence a degree of overlap between regions of higher iron signal and regions of higher bacterial abundance, notably at 17.75S, 17.4S, 17.2S, and 16.7S. Indeed, the region of highest measured microbial abundance (~2400m depth at ~17.4S) is spatially congruent with the highest iron concentrations (~2500m at 17.4S).

Graphically, the relationship between iron concentration and bacterial abundance is less clear, with a variable distribution above ~400nM tFe concentrations (Figure 7 A).

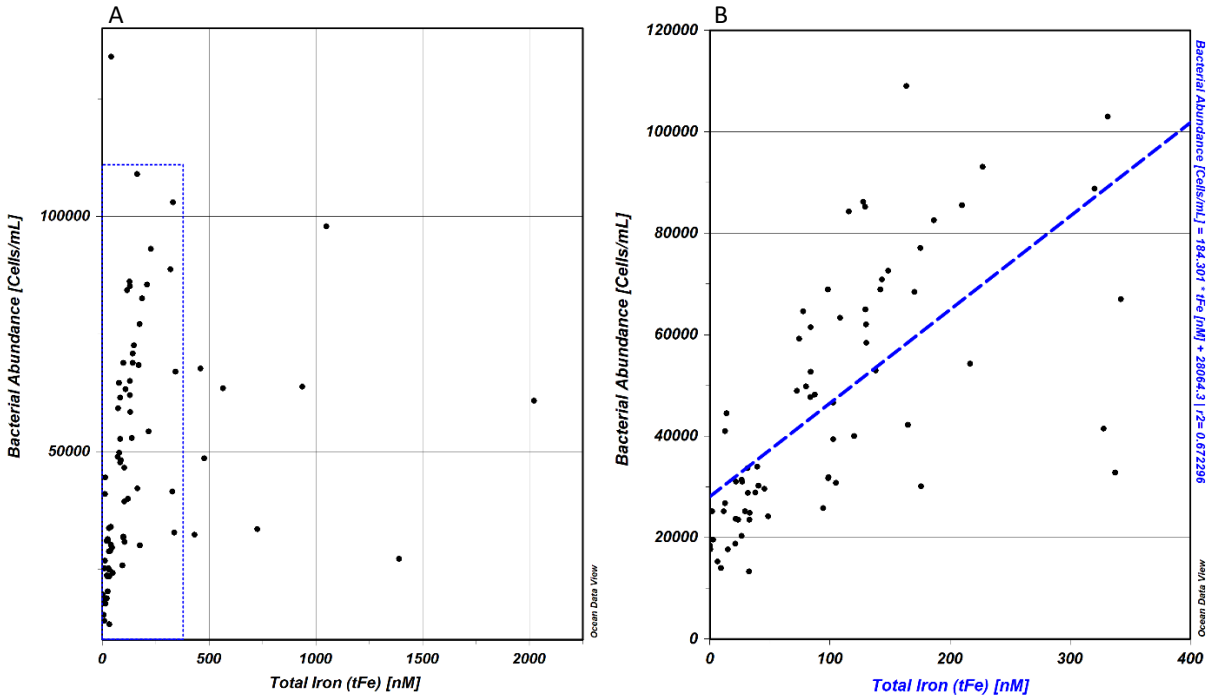

Figure 7: *Scatter and regression analysis of the distribution of total iron [nM] and bacterial abundance [Cells/mL], and region of majority of data clustering (blue dashed square: Iron Threshold = Average + 1 Standard Deviation)* ***(A)****. Bounding analysis to the majority clustering range, iron and bacterial abundance are clearly positively related (blue dashed least squared means trendline) with an* r^2 *value of 0.67* ***(B)****.*

A relationship between total iron and bacterial abundance is apparent within the lower *trace* concentrations of iron (Figure 7 B). Focusing the analysis within the blue rectangle, which bounds the majority of data clustering (~ Iron Average + 1 Standard Deviation), total Iron explains 67% of the variance in bacterial abundance measurements (~ Iron Average + 1 Standard Deviation).

Similar trace-patterns (low-concentration relationships) were also determined for Methane (CH_4) and Manganese (Mn) sampling (Figure 8) over a similar bounding region (~ CH_4, Mn Average Value + 1 Standard Deviation). Validation of this bounding region was assessed using descriptive statistics (Table 1).

					~ Upper Threshold
	Average	**Median**	**St.Dev.P**	**Max Value**	**Avg + 1 St.Dev.P**
Bacterial Abundance [cells/mL]	48377	41532	28576	164907	**76953**
tFe [nM]	133	74	235	2022	**368**
tMn [nM]	28	15	47	321	**75**
CH_4 [nM]	3	2	3	25	**6**

Table 1: Descriptive statistics and assessment of upper threshold for trace-concentration ranges for graphical (scatter) analyses.

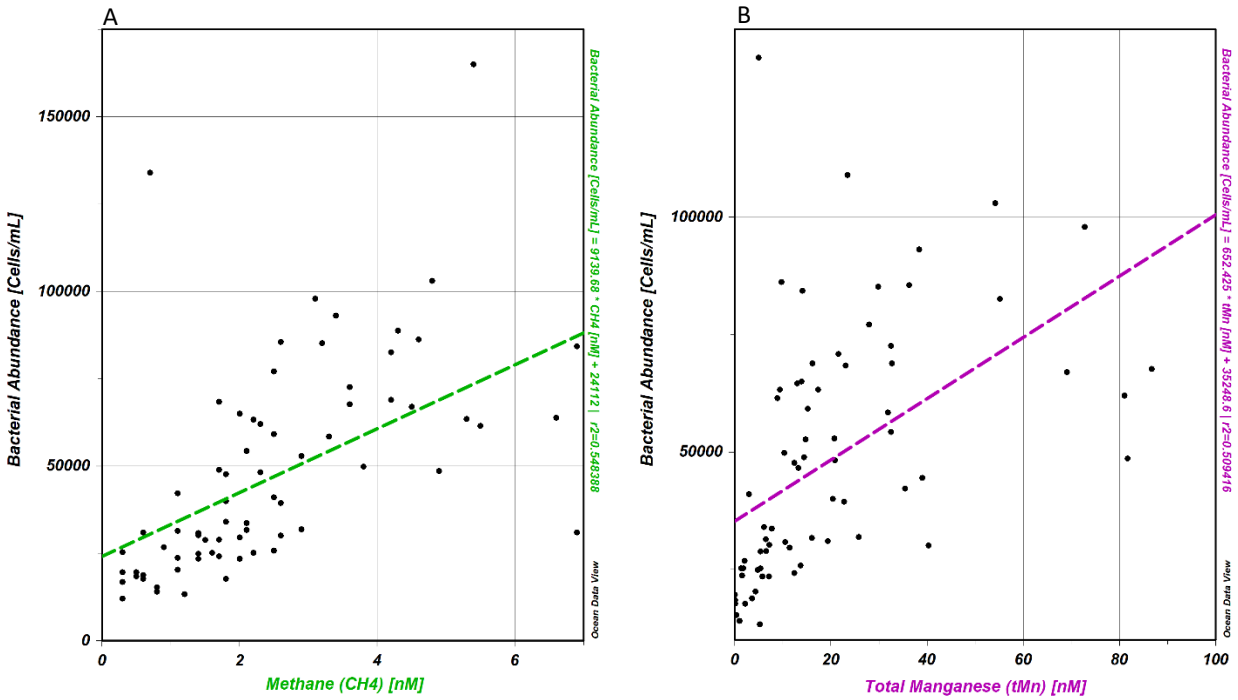

Figure 8: *Scatter and regression analysis of relationships between bacterial abundance and Methane (CH_4) [nM]* ***(A)****, and bacterial abundance and total manganese (tMn) [nM]* ***(B)****.*

Over the trace-concentration range, methane concentration could explain 55%, and total manganese concentration could explain 51% of the variance in bacterial abundance measurements.

Attempting to disentangle the trace-metal controls of growth limitation, I statistically evaluated the covariance of manganese and iron with respect to bacterial abundance (Figure 9).

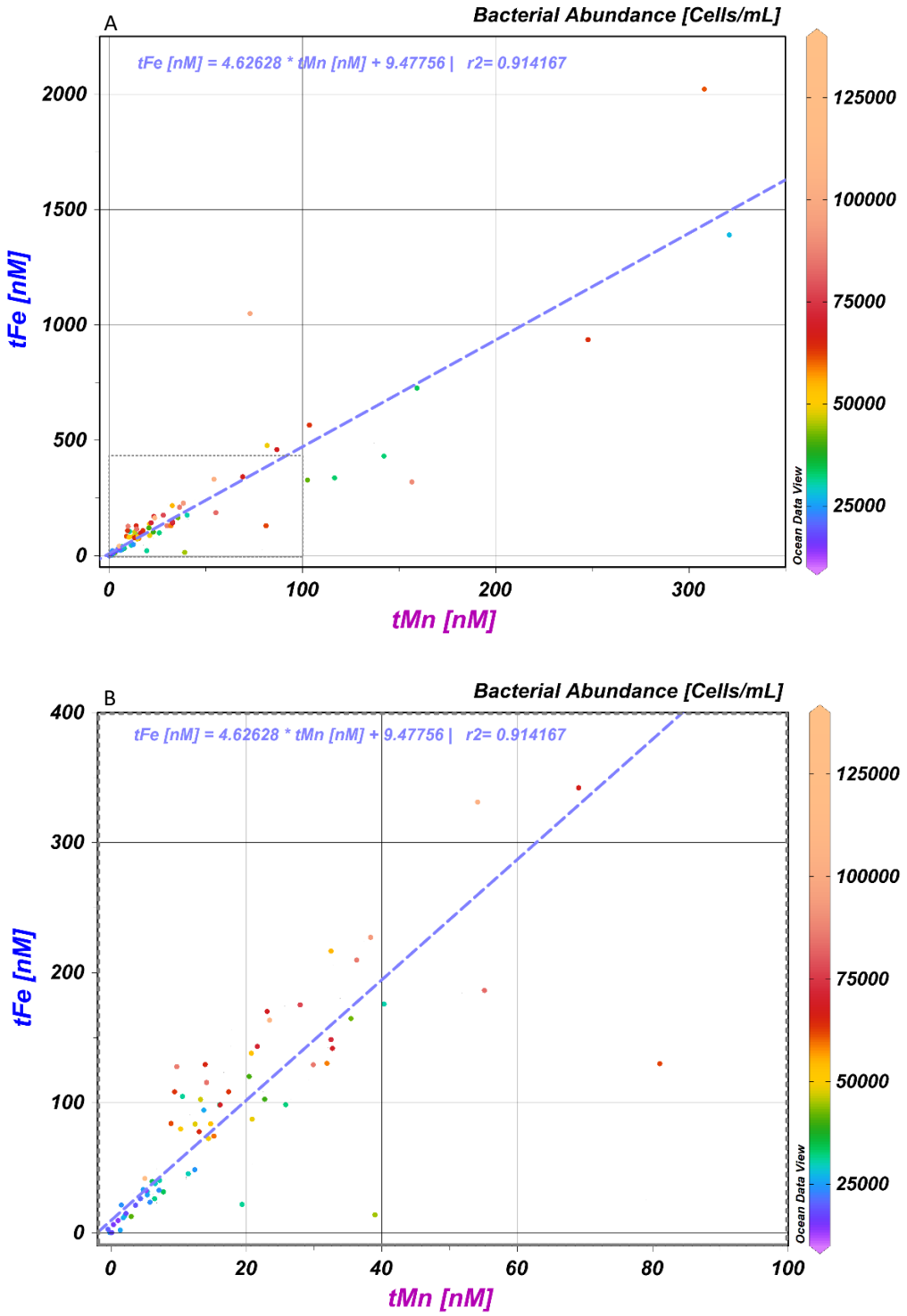

Figure 9: *Covariance between total iron and total manganese* ***(A)****, and combined impacts on bacterial abundance* ***(B)****. Data colors denote bacterial abundance in cells/mL. The blue dashed trendline describes the relationship between total iron and total manganese, determined in panel A over the full data range. Impacts on bacterial abundance (over the trace-concentration range; ~Average Value + 1 Standard Deviation for both tFe and tMn) is displayed by the dotted grey rectangle and the plot is constrained to this region in panel B.*

The trace-metal tFe:tMn ratio was 4.6:1 across all vent sites ($r^2_{tFe:tMn}$ = 0.91; Figure 9 A). Constraining to the trace concentration range, there is an increasing gradient in bacterial abundance as trace metal concentrations increase along the 4.6:1 tFe:tMn trend (Figure 9 B).

Discussion:

Predictive Value of ORP:

The absence of statistical relationship between bacterial abundance and ORP, and total iron and ORP suggest that the sampling approach, while appropriate for targeting plume signals, did not provide a strategic approach for sampling high iron nor high bacterial abundance water samples. This analysis was conducted utilizing discrete bottle-data (ORP signal at the moment of niskin bottle firing), which has the potential to miss key ORP signals due to sensor hysteresis or sampling variability. Since ORP signal specifically looks at the rate of change of the ORP sensor, discrete data with significant gaps between datapoints can miss key signals. The accuracy of the ORP's derivative (ORP Change) will be superior for the continuous dataset compared to the discrete bottle data. This method was employed because discrete bottle-data was the only available ORP data at the time of analysis, but further research is proposed to improve the ORP analysis using continuous rosette data once it is available. The higher resolution ORP data might not significantly impact the established relationship with bacterial abundance, given the above results, but would increase the confidence in my findings.

Trace-Metal Limitation of Microbial Growth:

To assess the impact of trace-concentrations of nutrients on microbial growth, I limited my analysis to a range of low-nutrient concentrations, which included the majority of the collected data. Limiting my statistical analyses to this trace-concentration range (~ Average Value + 1

Standard Deviation) is reasonable based on first principles, since iron often limits growth in diverse marine environments, and would likely limit growth over its lowest concentrations. One explanation is that above ~400nM tFe, another nutrient becomes limiting which terminates the clear iron-abundance relationship established over the 0 to 400nM tFe range. Further work is proposed to analyze nutrient data (collected on RR2106, but not processed by the time of this report) to assess whether other nutrients (like sulfides) could be limiting in samples above 400nM tFe. Once nutrient data is processed, similar analyses as presented here could be performed using other key micronutrients to assess whether variation in bacterial abundance above ~400 nM tFe can be explained. Additionally, I propose further research to perform log-regression analysis of the growth relationship to be more consistent with established biochemical kinetics models (like Monod Growth Kinetics) which describe nutrient uptake and microbial growth dynamics. A repetition of the existing analyses presented above using Python's Seaborn package would allow for this logistic regression to improve mechanistic accuracy of in-situ kinetics. Additionally, total iron and total manganese were utilized as a primary first-level assessment of relationship. I propose conducting a similar analysis utilizing only dissolved iron and dissolved manganese concentrations, since dissolved chemical species are more bioavailable than particulate chemical species (which are included in tFe and tMn counts).

Implications of Trace-Metal Covariance:

The strong relationship (and covariance) determined between tFe and tMn in the context of bacterial growth complicates conclusions regarding which nutrient is actively limiting growth. Assessing trace-metal nutrients in combination (Figure 8) allows us to propose nutrient limitation by trace-metals, since bacterial abundance increases with increasing concentrations of both tFe and tMn. Data exhibiting low tFe concentrations and higher tMn concentrations (and departing

from the established 4.6:1 tFe:tMn relationship) could suggest that tFe is actively limiting growth (as hypothesized by precedence of Fe limitation in the global oceans; Moore et al. 2013) since bacterial abundance at those points remain low despite higher Mn concentrations. But insufficient data exists at these specific chemical ratios to confidently support this assessment. At the time of this analysis, nutrient data (like sulfides and other core micronutrients) were not yet processed, but I propose further research to integrate other nutrients into this analysis. Additionally, incubation experiments could be performed to parametrically elucidate possible mechanism of nutrient limitation in vent plumes by controlling concentrations of key nutrients.

Subsequent work will help to elucidate the community structure and metabolic and molecular mechanisms of iron uptake and impacts on bioavailability through metagenomic analysis of siderophore genetic potential (Tang et al. 2013). Metagenomic sampling collects all of the organisms in a water sample and extracts all of the genomes, compiling them into a community-scale genomic dataset (Bik 2014). The FCM data described here is essential to this genomic work because it will establish the biomass in a given sample, allowing for estimation of theoretical DNA volume yield for sequencing. The metagenomic analysis will allow for further analysis of genetic potential for siderophore (and other key biomolecule) production, which will complement the first-order relationship between abundance and nutrient concentration established here. This will allow me to add layers of community structure and metabolic strategy to this analysis to assess how different vents with potentially distinct chemical and biological signatures behave.

Conclusions:

Global biogeochemical cycling of key micro- and macro-nutrients is essential to maintaining earth's habitability. I investigated the relationship between trace-chemicals (Fe, Mn, CH_4) and

microbial growth in deep sea hydrothermal vents, and assessed potential growth limitation by low environmental concentrations of these key nutrients. I find that ORP is related to plume signal, but is not predictive of bacterial abundance nor iron concentration. Additionally, total iron explains 67% of the variance in bacterial abundance data at trace concentrations, consistent with hypotheses regarding nutrient limitation. Furthermore, bounding my analysis to the same trace-concentration range (~Upper Threshold = Sample Average + 1 Standard Deviation), I find that methane and total manganese also exhibit bacterial abundance relationships, explaining 55% and 51% of the variance respectively. I also find that tFe:tMn ratios were consistent across all sampled vents, evidencing a 4.6:1 ratio with an r^2 of 0.91. Additionally, constrained over the trace-concentration range for both tFe and tMn, bacterial abundance increased with increasing concentrations of both trace-metals. These findings suggest that microbial abundance in vent plumes could be partially explained by trace element and methane distributions. Data which deviates from the established 4.6:1 tFe:tMn relationship suggest that Fe could be controlling this limitation as bacterial abundance remains low despite manganese enrichment, however additional data is required to statistically support this assessment. Continued research is proposed to further our understanding of nutrient limitation and disentangle whether these key nutrients are covarying with other biochemical controls impacting microbial growth and metabolism in these complex and dynamic deep-sea ecosystems.

Acknowledgements:

Thank you to the following for your insights and support:

UW Center for Environmental Genomics:

Dr. Robert Morris

National Science Foundation RR2106:

Dr. Randie Bundy and the UW Oceanography Bundy Lab Group,

Chief Scientists Dr. Joseph Resing and the RR2106 Science Team,

Captain David Murline and the Crew of the R/V Roger Revelle,

UW Oceanography Senior Thesis Teaching Team:

Dr. Ginger Armbrust,

Dr. Mark Warner,

Dr. Kathy Newell,

Dr. Rick Keil,

Dr. William Wilcox,

and the Senior Thesis student body for peer review

References*:*

Bik, H. M. 2014. Deciphering Diversity and Ecological Function From Marine Metagenomes. The Biological Bulletin **227**: 107–116. doi:10.1086/BBLv227n2p107

Birchill, A. J., N. T. Hartner, K. Kunde, and others. 2019. The eastern extent of seasonal iron limitation in the high latitude North Atlantic Ocean. Sci Rep **9**: 1435. doi:10.1038/s41598-018-37436-3

Boyd, P. W., K. R. Arrigo, R. Strzepek, and G. L. van Dijken. 2012. Mapping phytoplankton iron utilization: Insights into Southern Ocean supply mechanisms: Southern Ocean Fe utilization and supply. J. Geophys. Res. **117**: n/a-n/a. doi:10.1029/2011JC007726

Genitsaris, S., S. Monchy, J. Denonfoux, S. Ferreira, K. Ar. Kormas, T. Sime-Ngando, E. Viscogliosi, and U. Christaki. 2016. Marine microbial community structure assessed from combined metagenomic analysis and ribosomal amplicon deep-sequencing. Marine Biology Research **12**: 30–42. doi:10.1080/17451000.2015.1084425

Moore, C. M., M. M. Mills, K. R. Arrigo, and others. 2013. Processes and patterns of oceanic nutrient limitation. Nature Geosci **6**: 701–710. doi:10.1038/ngeo1765

Resing J.A., P.N. Sedwick, C.R. German, W. J. Jenkins, J.W. Moffett, B.M. Sohst, A. Tagliabue, 2015. Basin-scale transport of hydrothermal dissolved metals across the South Pacific Ocean. Nature. **523:** 200-203

Statham, P., C. German, and D. Connelly. 2005. Iron (II) distribution and oxidation kinetics in hydrothermal plumes at the Kairei and Edmond vent sites, Indian Ocean. Earth and Planetary Science Letters **236**: 588–596. doi:10.1016/j.epsl.2005.03.008

Tagliabue, A., A. R. Bowie, P. W. Boyd, K. N. Buck, K. S. Johnson, and M. A. Saito. 2017. The integral role of iron in ocean biogeochemistry. Nature **543**: 51–59. doi:10.1038/nature21058

Tang, K., K. Liu, N. Jiao, Y. Zhang, and C.-T. A. Chen. 2013. Functional Metagenomic Investigations of Microbial Communities in a Shallow-Sea Hydrothermal System B.A. White [ed.]. PLoS ONE **8**: e72958. doi:10.1371/journal.pone.0072958

Twining, B. S., and S. B. Baines. 2013. The Trace Metal Composition of Marine Phytoplankton. Annu. Rev. Mar. Sci. **5**: 191–215. doi:10.1146/annurev-marine-121211-172322

Zhao, F., and V. B. Bajic. 2015. The Value and Significance of Metagenomics of Marine Environments. GPB **13**: 271–274. doi:10.1016/j.gpb.2015.10.002